AIAA SciTech Forum
23-27 January 2023, National Harbor, MD & Online
AIAA SCITECH 2023 Forum

10.2514/6.2023-2156

Multi-Agent Passivity-based Control for Perception-based Guidance

Aditya Deole*, Shahriar Talebi†, Spencer Kraisler‡, Niyousha Rahimi§, Mehran Mesbahi¶
Dept. of Aeronautics & Astronautics, University of Washington, Seattle, Washington 98195, USA

Saptarshi Bandyopadhyay‖, Vinod Gehlot**, William Seto††, and Amir Rahmani‡‡
Jet Propulsion Laboratory, California Institute of Technology, Pasadena, California 91109, USA

Jonathan Becktor§§
Technical University of Denmark, Lyngby, Denmark

This work presents a passivity-based control approach for tracking an uncooperative target spacecraft within the ego camera center via attitude guidance stabilization. A camera and ML based state estimation are used to generate target pose and position estimates in ego camera frame in a photo-realistic simulation environment. The control approach is robust to noisy observations and uncertainties in the perception map. The sensing error is modelled using sector bounded nonlinearities and passivity conditions on the perception map. We show that feedback interconnection with CNN based observation is stable under set constraints and derive an optimal control law for the corresponding feasible set. The modular nature of this passivity-based synthesis also allows us to incorporate observations from multiple ego spacecraft, and subsequently, use a consensus protocol on the target position in order to improve the tracking performance.

I. Introduction

Satellite proximity operation is an important area for space-based autonomous applications in low Earth orbit (LEO). Coordination tasks is a prime example for such autonomous operations, carried out between multiple spacecraft through information sharing over a network. When information about the target is known or communication has been established amongst the agents, coordination can be achieved with high precision [1]. Certain coordination tasks, of recent interest, like capturing space debris or landing a probe on an asteroid, pose a new set of challenges involving coordination with an otherwise uncooperative celestial body [2]. We look at a specific scenario where it is desired to track uncooperative target spacecraft and align it with the camera of the ego spacecraft. We will look at the design of a robust passivity-based controller for this target-ego alignment problem and extend it to multi-agent settings in order to improve the tracking/guidance performance. Here the target spacecraft is an uncooperative satellite in LEO. The (multiple) ego spacecraft we consider are initially "parked" in a passive elliptical orbit around the target with an estimate of the target direction. The estimation task of relative pose of the target with respect to ego is achieved through a Convolution Neural Network (CNN). The CNN takes in high-resolution images and determines the relative position and orientation (pose) of the target. Recently, some works have shown that highly reliable estimates of the object pose can

*Ph.D. Student, Robotics, Aerospace and Information Networks (RAIN) Lab, University of Washington, Seattle, WA 98195, USA,
†Postdoctoral Researcher, Robotics, Aerospace and Information Networks (RAIN) Lab, University of Washington, Seattle, WA 98195, USA,
‡Ph.D. Student, Robotics, Aerospace and Information Networks (RAIN) Lab, University of Washington, Seattle, WA 98195, USA,
§Ph.D. Student, Robotics, Aerospace and Information Networks (RAIN) Lab, University of Washington, Seattle, WA 98195, USA,
¶Professor, Robotics, Aerospace and Information Networks (RAIN) Lab, University of Washington, Seattle, WA 98195, USA **AIAA Associate Fellow**
‖Robotics Technologist, Mobility and Robotic Systems Section, Jet Propulsion Laboratory, California Institute of Technology, 4800 Oak Grove Drive, Pasadena, California 91109, USA.
**Postdoctoral Researcher, Mobility and Robotic Systems Section, Jet Propulsion Laboratory, California Institute of Technology, 4800 Oak Grove Drive, Pasadena, California 91109, USA.
††Robotics Technologist, Mobility and Robotic Systems Section, Jet Propulsion Laboratory, California Institute of Technology, 4800 Oak Grove Drive, Pasadena, California 91109, USA.
‡‡Group Supervisor, Maritime and Multi-Agent Autonomy Group, Mobility and Robotic Systems Section, Jet Propulsion Laboratory, California Institute of Technology, 4800 Oak Grove Drive, Pasadena, California 91109, USA. **AIAA Life Member**
§§Ph.D. Student, Technical University of Denmark, Anker Engelunds Vej 1 Bygning 101A, 2800 Kgs. Lyngby, Denmark,

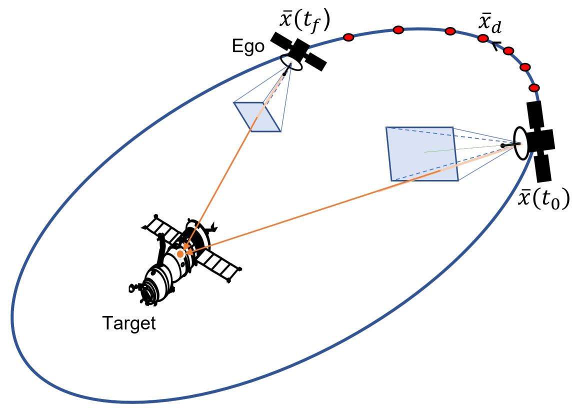

Figure 1 :Tracking a target satellite in a passive relative orbit. The ego spacecraft initializes a trajectory where it tracks the target to ego's camera center while cruising in the passive orbit.

be made directly from images; application specific to satellite pose have also been demonstrated [3][4][5]. These types of architectures extract features from an RGB image and a convolution of those features is used to build a 6D pose of the object. These networks are competitive with the conventional sensory based observations and require only a monocular camera for observations. Thus, these architectures are of interest to be used in real time guidance and control loops.

Our contribution addresses key challenges in embedding CNN-based modules in the guidance and control loop. In particular in this work, we propose,

- A passivity-based controller that operate with uncertain observations, guaranteed to result in a passivity-short stable system.
- Given passivity constraints, we then design an optimal control law for a given quadratic cost using zeroth order optimization.
- We then proceed to extend the controller to accommodate for information from neighbouring, and generally passive, agents.

The problem setup considers an uncooperative tumbling target satellite in a (circular) low Earth orbit; the ego spacecraft on the other hand is in a relative passive orbit with respect to the target. This is an elliptical orbit as shown in Fig-1 in the target's Hill's frame [6], [7].

target tracking problems in this setting have been studied in detail through various approaches [8]. Robust control using Lyapunov theory has been well studied in this domain [9], where attitude specific Lyapunov functions are used to derive stability conditions. Extensions of the Lyapunov approach include passivity based approaches that we examine in this work. The passivity approach facilitates interconnection between the sub-systems and analyze the stability of the overall system [10][11][12][13].

Through the passivity approach we will deal with nonlinear uncertain observations from the perception map. Conventionally, passivity-based control design under noise/uncertainties leads to high gain controllers [14]. Stability and optimality for this approach has been studied by Tsiotras, where optimal solutions are obtained using Hamilton-Jacobi theory via a modified control law with a quadratic cost [15]. In our approach, will look at a constrained problem and derive linear controllers for the guidance loop. Using a state and input based quadratic cost, we then proceed to optimize on the feasible set of control gains.

For the satellite attitude control problem we have two independent dynamical systems for the ego spacecraft, that are passive as well as lossless. The inspiration to use passivity comes from the fact that for a feedback interconnection of passive systems, under conditions such as observability and strict passivity, the overall system can be ensured to be passive and stable [16]. We further build on this relation to connect multiple passive systems and then propose a consensus-based process to improve the corresponding estimates for distributed architectures.

Another motivation for using passivity comes from the fact that a generalized notion of passivity can be used to describe our sensor characteristics. Our ego spacecraft uses neural networks which take image inputs and provides relative locations of target spacecraft in the camera frame as an output. A detailed overview of this simulation setup, and description on NN architecture have been discussed in [17]. There, we also discuss a characteristics of the sensor specific to the environment. Through an exhaustive analysis on input-output characteristics of CNN we find that object pose measurements have a state dependent error profile and have dependence on environment factors such as illumination and celestial background. There have been works that use some approaches using NN in robust control loops by bounding NN outputs using SDPs [18][19] or use Lipschitz constants of individual layers to bound outputs [20]. Another approach is to modify learning and control such that the inputs stay close to a nominal trajectory and NN output is slope bounded near these trajectories [21]. We consider an extension to this approach by modeling the error near nominal trajectory as time varying and state dependent with some residual due to uncertainties. For a fixed trajectory this model has been used in the feedback to design a robust controller using funnel synthesis [17].

Instead of using a trajectory based setup to define the error profile, we look at passivity of neural network which can be used to characterise a generalized error model. We can use this model independent of trajectories. Intuitively we can see that for the perception map, barring any outliers or adversarial noise, the direction of target position measured is roughly the same as true target Position as seen in Fig-3b. This directionality of input-output means that any extra energy created by the perception map, that induces error, might be bounded. This perception map would constitute a lossless system if there was no error and thus no energy was created. To verify this directional nature of measurements and put a bound on the noise characteristics, we test the data on the perception map's feasible state space. Empirically we see in our simulations that perception map output is sector bounded along the input direction outside of an ellipse around the origin as seen in Fig-4a. Thus input-output has a generalized passivity-short nature. We define the passivity conditions and error bounds for the CNN empirical analysis and exploit this passive nature while designing the control law.

Given that we establish a feedback system with the perception map, the entire system can be defined as passive by selecting appropriate input-output pair and storage function. Now for multi-agent setup, for each ego spacecraft in the passive orbit around target, we can associate a passive system. These passive systems can then be used in a distributed setup where relative attitude measurements from each ego spacecraft is communicated to a candidate ego in its frame and these measurements can be used to converge to a consensus on the relative measurement as opposed to measurements from the single ego spacecraft. Given that consensus generally improves estimation, one can put stricter bounds on error and use a more aggressive controller for the distributed scenario.

In the following sections, we discuss the problem formulation and simulation framework, as well as the setup for the multi-agent state estimation.

II. Problem Setup

A. Simulation and Estimation Setup

Relative state estimation for the target-ego problem can be reliably achieved through conventional sensing methods and sensor fusion. We specifically focus on using images and extraction of features through CNN for this problem. The CNN-based pose estimation methods, either use direct regression [22] of position and attitude quaternions from image or approaches that regress onto key-points [23] on the target. We have observed that for problems with approximately known target geometry, key-point methods perform better [24]. We use a custom architecture, developed at JPL [24], that uses a segmentation network to isolate the target; this is then followed by a key-point network that maps the pose. The simulation setup we designed consists of a astrodynamics simulator module that uses Basilisk [25]. A separate visualisation tool is developed in Unreal Engine (UE) to provide photo-realism to our observations. Celestial and ego-target current state data is sent to UE and a camera snapshot is recorded. The image is processed through the CNN module and relative pose feedback is used to assign the control back to Basilisk. The system structure is shown in Fig- 2. A modified version of end-to-end simulation pipeline is under development at JPL specifically for real time computation of multiagent spacecraft units. The pipeline is a modular so that scripts written in Python and C can be incorporated easily.

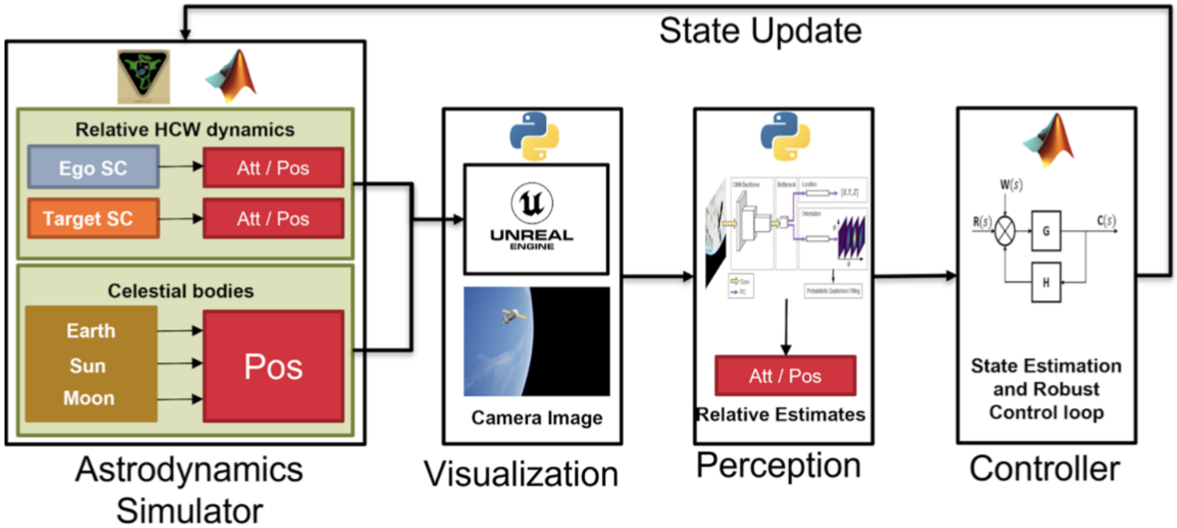

Figure 2 :Representation of System architecture showing the distinct modules. The Basilisk/Matlab based dynamics simulator initiates the trajectory, which is visualised in UE. Here the sensory information from ego spacecraft (image) is sent to the CNN module which estimates the relative pose. The control loop uses this measurement in feedback and gives input commands back to dynamics module. Multiple iterations of ego can run in this same setup for multi-agent simulations.

B. Modelling Perception map

We now go through error modelling for the perception map (pose CNN), by mapping its input-output characteristics. To define the perception map $\mathcal{H}$, we examine the relative dynamics between ego and target. Given a relative target position $\boldsymbol{x}_t \in \mathbb{R}^3$ in ego's camera frame, we define a desired ego attitude that needs to track the target to ego camera center as $\boldsymbol{q} \in \mathbb{R}^3$ (the attitude is represented by Modified Rodriguez Parameters (MRPs)). When we refer to the relative attitude $\boldsymbol{q}$ we will discuss the tracking error between target in ego's camera frame to the center of the camera frame ($\boldsymbol{q}$ will be zero when target and ego camera center are aligned) as seen in Fig-3b. We define our non-linear dynamics ($\dot{\boldsymbol{q}}, \dot{\boldsymbol{\omega}}$) in these relative ego attitude terms as well. The figure below shows a representation of the perception map where for a true relative attitude $\boldsymbol{q}$ an image $z(\boldsymbol{q})$ is generated and the CNN provide a noisy/uncertain estimate of the relative attitude from the image.

Thus the perception map is defined as $\tilde{\boldsymbol{q}} = \mathcal{H}(\boldsymbol{q})$, where $\tilde{\boldsymbol{q}}$ is the noisy measurement of the true relative ego attitude. In order to generalize the map over the feasible state space of relative pose between ego and target, we utilize a PID controller to generate a basic tracking trajectory. Then we initialise multiple trajectories spanning the feasible relative ego state space corresponding to possible target positions in the ego camera frame. Celestial variables are randomised over the trajectories, i.e., the Earth position relative to ego and possible Sun angles are varied over the trajectories. This provides the dataset for an empirical model for input-output characteristics of the perception map as seen in Fig-4a. We model the map as represented by Fig-4b. Here we see that we can define a set in the neighborhood of the origin outside of which sector bounded passivity is valid. The maximum error in measurement $||\tilde{\boldsymbol{q}} - \boldsymbol{q}||$ is also bounded due to mission constraints. The definitions for these constraints on the perception map shown in Fig-4b are discussed in section II.D:2.

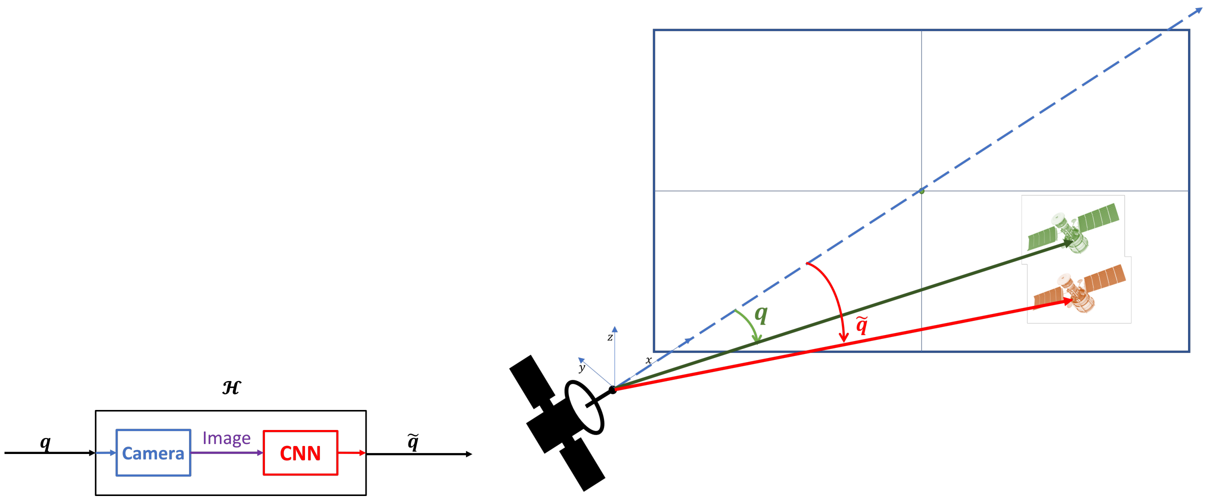

(a) **(b)**

Figure 3 :(a) The perception map shown in the figure maps true relative attitude q to its perceived measurement $\tilde{q}$. (b) Depicts the true target position in the ego camera frame in green, where q represents the relative attitude of ego to align the target with the camera center as shown. Similarly, measured position is shown in red and the corresponding relative attitude measurement is $\tilde{q}$

.

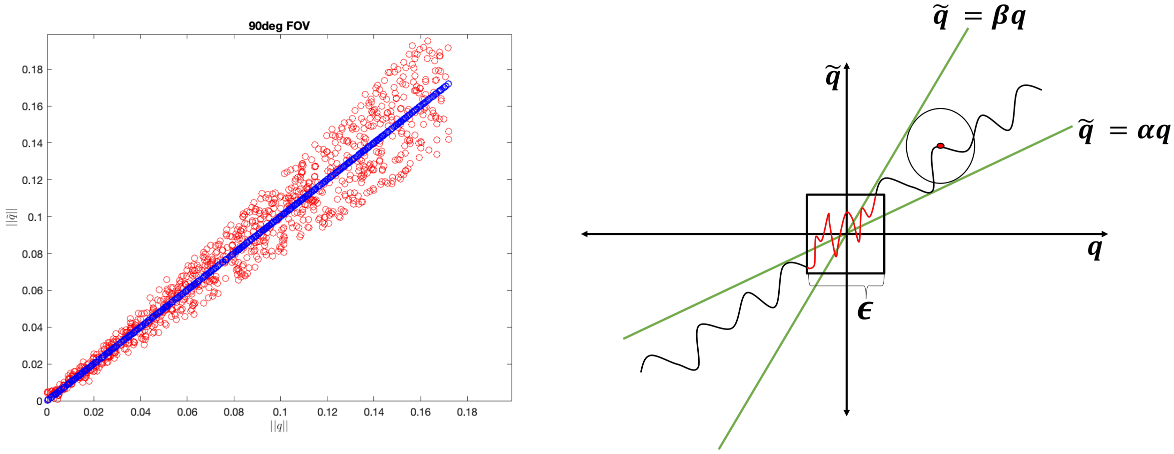

(a) **(b)**

Figure 4 :(a) Empirical data showing input-output characteristics of ego's relative attitude norm i.e. $||q||$ vs $||\tilde{q}||$ with outlier and averaging filter. Data shows state dependence of the perception error as for larger $||q||$ we see higher deviation in measurement $||\tilde{q}||$. The plot also shows loss of passivity near the origin. (b)ϵ-ball representation of the error model used to define constraints. In the neighborhood of origin, outside this ϵ-ball set we show sector bounded nature of the perception map.

C. Passivity feedback problem setup

The dynamics we discuss here are the relative attitude dynamics $\boldsymbol{q}$ with respect to the desired attitude for tracking and the angular rate error $\boldsymbol{\omega}$. It is desired to develop a stable tracker using feedback from the perception map. Further, we want to define this system with a tracking controller as passive overall against an input-output pair and a storage function V. In this direction, we first examine the baseline system made up of a passive attitude dynamic system (2) and a passive attitude rate (1) system.

Now consider the systems [12]:

$$J\dot{\omega} = (J\omega) \times \omega + u \tag{1}$$
$$\dot{\boldsymbol{q}} = G(\boldsymbol{q})\omega \quad , \tag{2}$$

where, $G(\boldsymbol{q}) = \frac{1}{2}\left[I_3(\frac{1-\boldsymbol{q}^T\boldsymbol{q}}{2}) + S(\boldsymbol{q}) + \boldsymbol{q}\boldsymbol{q}^T\right]$ and $S(\boldsymbol{q}) = \begin{bmatrix} 0 & -q_3 & q_2 \\ q_3 & 0 & -q_1 \\ -q_2 & q_1 & 0 \end{bmatrix}$

Let us now define the passivity properties for these subsystems.

D. Passivity Definitions for Attitude stabilization

For the attitude stabilization problem, passivity between subsystems has been studied thoroughly [12][26]. We will build upon the following definitions for our case where the input is generated from a network of noisy observers. A general definition of passivity has been defined in VII.A.

- System (1) is passive for input $\boldsymbol{u}$ and output $\boldsymbol{\omega}$.
  Proof: For a candidate storage function $V_1(\omega) = \frac{1}{2}\boldsymbol{\omega}^T J\omega$, we take the derivative along the trajectories as $\dot{V}_1 = \boldsymbol{\omega}^T u \rightarrow \dot{V}_1 \leq \boldsymbol{\omega}^T u$, i.e., the system is lossless-passive for storage function V_1 and input-output pair $u, \boldsymbol{\omega}$.

- System (2) is passive for input $\boldsymbol{\omega}$ and output $\boldsymbol{q}$.
  Proof: For a candidate storage function $V_2(\boldsymbol{q}) = 2\ln(1 + \boldsymbol{q}^T\boldsymbol{q})$, we take the derivative along the trajectories as $\dot{V}_2 = \boldsymbol{q}^T\boldsymbol{\omega} \rightarrow \dot{V}_2 \leq \boldsymbol{q}^T\boldsymbol{\omega}$, i.e., the system is lossless-passive for storage function V_2 and input-output pair $\boldsymbol{\omega}, \boldsymbol{q}$.

We now use a general passivity result which states that feedback interconnection of a strictly passive system and a passive system leads to a stable system[16]. Stabilization of attitude rate system using feedback connection can be achieved through a linear feedback law, Theorem:1.

Definition 1. *The system (1) with $\boldsymbol{u} = -k_\omega\boldsymbol{\omega} - \boldsymbol{\nu}$ is strictly passive for input ν and output $\boldsymbol{\omega}$*

Proof: For $V_1(\omega) = \frac{1}{2}\boldsymbol{\omega}^T J\omega$, Differentiating along the trajectories gives: $\dot{V}_1(\omega) = \boldsymbol{\omega}^T J\dot{\boldsymbol{\omega}} = -k_\omega||\boldsymbol{\omega}||^2 + \boldsymbol{\omega}^T\boldsymbol{\nu}$ which is strictly passive with dissipation rate $-k_\omega||\boldsymbol{\omega}||^2$

Now the output of attitude dynamic system $\boldsymbol{q}$ is taken as the input $\boldsymbol{\nu}$ to system (2) st $\boldsymbol{u} = -k_\omega\boldsymbol{\omega} - \boldsymbol{\nu}$. Thus we have an interconnection of a strictly passive subsystem and a passive subsystem.

Definition 2. *The control law $\boldsymbol{u} = -k_\omega\boldsymbol{\omega} - k_q\boldsymbol{q}$ for $k_\omega > 0, k_q > 0$ globally stabilizes system (1) (strictly passive) and system (2)(passive) for a radially unbounded storage function.*

Proof: Here, take the candidate storage function as $V(\boldsymbol{\omega}, \boldsymbol{q}) = V_1(\omega) + k_q V_2(\boldsymbol{q}) = \frac{1}{2}\omega J\omega + 2k_q\ln(1 + \boldsymbol{q}^T\boldsymbol{q})$. Differentiating along the trajectories:

$$\begin{aligned}\dot{V} &= \omega J\dot{\omega} + 4k_q\frac{\boldsymbol{q}^T\dot{\boldsymbol{q}}}{(1 + \boldsymbol{q}^T\boldsymbol{q})} \\ &= \boldsymbol{\omega}^T u + k_q\boldsymbol{q}^T\boldsymbol{\omega} = -k_\omega||\boldsymbol{\omega}||^2 \leq 0\end{aligned}$$

Thus for this aforementioned Lyapunov function the system is asymptotically stable using LaSalle's invariance principle [16].

III. Passivity based control for non linear observations

A. Feedback interconnection under a noisy observer

As shown in the setup in **Definition 1**, we have a strictly passive system (1) for input ν and output $\boldsymbol{\omega}$ where $\boldsymbol{u} = -k_\omega \boldsymbol{\omega} - \boldsymbol{\nu}$. Now for the case with a measurement through the perception map, the input to the system (2) is $\boldsymbol{u} = -k_\omega \boldsymbol{\omega} - k_q \tilde{\boldsymbol{q}}$. We will use this noisy feedback and provide a systematic means of dealing with the error.

Expanding on **Definition 2** we take the candidate Lyapunov function for the feedback system as $V = V_1 + k_q V_2$ for the above input where:

$$\dot{V} = \boldsymbol{u}^T \boldsymbol{\omega} + k_q \boldsymbol{q}^T \boldsymbol{\omega} \tag{3}$$

$$= (-k_\omega \boldsymbol{\omega} - k_q \tilde{\boldsymbol{q}})\boldsymbol{\omega} + k_q \boldsymbol{q}^T \boldsymbol{\omega} \tag{4}$$

$$= -k_\omega ||\boldsymbol{\omega}||^2 - k_q (\tilde{\boldsymbol{q}} - \boldsymbol{q})^T \boldsymbol{\omega} \tag{5}$$

Here for stability we say that a necessary condition for $\dot{V} \le 0$ is $||\boldsymbol{q}|| > \epsilon$,$||\boldsymbol{\omega}|| > \Omega$ and $||\tilde{q} - q|| < \delta$ for some $\epsilon, \Omega, \delta > 0$. We arrive at this condition for stability as $||\boldsymbol{\omega}||^2$ is always positive but the second term $(\tilde{\boldsymbol{q}} - q)^T \boldsymbol{\omega}$ could be negative and there are no feasible controller gains if $||\boldsymbol{\omega}|| << ||\tilde{\boldsymbol{q}} - \boldsymbol{q}||$. This gives a lower bound on $\boldsymbol{\omega}$ and an upper bound on the error. Moreover obtain a lower bound condition on $\boldsymbol{q}$ from a passivity-short nature of the perception map discussed in following section. We can now say that if we stay outside a **zero state set** O the Lyapunov inequality defined below is feasible given that error is bounded (these bounds on error are discussed in the following section).

$$-k_\omega \boldsymbol{\omega}^T \boldsymbol{\omega} - k_q (\tilde{\boldsymbol{q}} - \boldsymbol{q})^T \boldsymbol{\omega} \le 0$$
$$k_\omega \boldsymbol{\omega}^T \boldsymbol{\omega} + k_q (\tilde{\boldsymbol{q}} - \boldsymbol{q})^T \boldsymbol{\omega} \ge 0$$

For the zero state set we define the control to be $u = 0$ and Lyapunov function to be $V(O) = 0$ and output $\tilde{\boldsymbol{q}} = 0$.

Now to analyze the constraint sets we transform the inequality into a matrix inequality for internal states of the system. In particular, we set $\boldsymbol{x} = [\tilde{\boldsymbol{q}} - \boldsymbol{q}, \boldsymbol{\omega}, \boldsymbol{q}, 1]$ such that the matrix inequality in terms of $\boldsymbol{x}$ corresponds to:

$$\begin{bmatrix} \tilde{\boldsymbol{q}} - \boldsymbol{q} \\ \boldsymbol{\omega} \end{bmatrix}^T \begin{bmatrix} 0 & k_q/2 \\ k_q/2 & k_\omega \end{bmatrix} \begin{bmatrix} \tilde{\boldsymbol{q}} - \boldsymbol{q} \\ \boldsymbol{\omega} \end{bmatrix} \ge 0\,, \tag{6}$$

$$\begin{bmatrix} \tilde{\boldsymbol{q}} - \boldsymbol{q} \\ \boldsymbol{\omega} \\ \boldsymbol{q} \\ 1 \end{bmatrix}^T \begin{bmatrix} 0 & k_q/2 & 0 & 0 \\ k_q/2 & k_\omega & 0 & 0 \\ 0 & 0 & 0 & 0 \\ 0 & 0 & 0 & 0 \end{bmatrix} \begin{bmatrix} \tilde{\boldsymbol{q}} - \boldsymbol{q} \\ \boldsymbol{\omega} \\ \boldsymbol{q} \\ 1 \end{bmatrix} \ge 0\,, \tag{7}$$

which gives us matrix inequality of the form $\boldsymbol{x}^T A_0 \boldsymbol{x} \ge 0$. Thus the set of stabilizable states is given by $\mathcal{X} = \{\boldsymbol{x} | \boldsymbol{x}^T A_0 \boldsymbol{x} \ge 0\}$ for all states outside the zero-state set. Thus we can write this stability condition as:

$$\forall \;\; ||\boldsymbol{q}|| > \epsilon \;\text{ and }\; ||\boldsymbol{\omega}|| > \Omega \;\Rightarrow\; \boldsymbol{x}^T A_0 \boldsymbol{x} \ge 0 \tag{8}$$

The conditions defining zero-set O in (8), can also be written as $\boldsymbol{x}^T A_1 \boldsymbol{x} \ge 0$ and $\boldsymbol{x}^T A_2 \boldsymbol{x} \ge 0$ as shown in VII.D.

Using LaSalle's invariance principle we can say that the control u is asymptotically stabilizing with respect to the zero-state set[16].

Note that the linear error we use here is applicable for small deviation between $\tilde{\boldsymbol{q}}$ and $\boldsymbol{q}$. For relatively small deviation, the linear error $(\tilde{\boldsymbol{q}} - \boldsymbol{q})$ represents a valid attitude representation near the origin. We empirically see deviation of the three orders of magnitude less than the current attitude and is small enough such that we can treat it as an error in estimation.

B. Constraint set for the perception map

In order to design a robust controller for the noisy observer setup, we define the perception map and impose state based constraints on $\tilde{\boldsymbol{q}}$ and a maximum bound on the measurement noise. The perception map is modelled as $\tilde{\boldsymbol{q}} = \mathcal{H}(\boldsymbol{q}) = \boldsymbol{q} + e$ as seen in Fig-4b. Empirically, through simulations, we obtain an input output characteristic for this map $\mathcal{H}$ shown by Fig-4a. We exhaustively search over the input space of the neural network and obtain performance bounds discussed below.

The behaviour of $\tilde{\boldsymbol{q}}$ is defined to follow the given necessary conditions for the controller to be stabilizing w.r.t. the zero-set:

1) We observe that near equilibrium i.e., for states $\boldsymbol{q} \approx 0$, the perception map has considerable residual error as shown by the graphical representation in Fig- 4b. Thus we define this mapping $\mathcal{H}$ as **passivity-short** w.r.t. input-output $\boldsymbol{q}$ and $\tilde{\boldsymbol{q}}$. We can write this as the desired behaviour $\boldsymbol{q}^T\tilde{\boldsymbol{q}} \geq 0$ under the constraint $||\boldsymbol{q}|| > \epsilon$.

2) Measurement through the perception map is **sector bounded**. The input-output characteristic of the NN has a property of being passive and sector bounded. This is a desirable property showing that tighter sector bounds means a lower perception error. This also captures the state dependence of the perception error. In a related work [17], we use a state dependent error model around a nominal trajectory. Here we capture the error for a more generalised case for all trajectories using passivity. Now, for region outside the zero state set we have the state dependent measurement error bounded by sectors:

$$\beta\boldsymbol{q}^T\boldsymbol{q} \geq \tilde{\boldsymbol{q}}^T\boldsymbol{q} \geq \alpha\boldsymbol{q}^T\boldsymbol{q} \ ,$$

that provides two separate constraints for upper and lower sector bounds as follows:

$$\beta\boldsymbol{q}^T\boldsymbol{q} - \tilde{\boldsymbol{q}}^T\boldsymbol{q} + \boldsymbol{q}^T\boldsymbol{q} - \boldsymbol{q}^T\boldsymbol{q} \geq 0 \tag{9}$$

$$-(\tilde{\boldsymbol{q}} - \boldsymbol{q})^T\boldsymbol{q} + (\beta - 1)\boldsymbol{q}^T\boldsymbol{q} \geq 0 \tag{10}$$

$$\tilde{\boldsymbol{q}}^T\boldsymbol{q} - \alpha\boldsymbol{q}^T\boldsymbol{q} + \boldsymbol{q}^T\boldsymbol{q} - \boldsymbol{q}^T\boldsymbol{q} \geq 0 \tag{11}$$

$$(\tilde{\boldsymbol{q}} - \boldsymbol{q})^T\boldsymbol{q} + (1 - \alpha)\boldsymbol{q}^T\boldsymbol{q} \geq 0. \tag{12}$$

3) The perception error and attitude is also **bounded from above** from mission constraints i.e., $||\tilde{\boldsymbol{q}} - \boldsymbol{q}|| \leq \delta$ and $||\boldsymbol{q}|| \leq \gamma$

The section VII.D shows representation of all these constraints in the form of matrix inequalities in the quadratic form discussed in the previous section. Finally, the assertion made for the observer is that any outlier and adversarial noise is rejected through an averaging filter.

C. Feasibility Analysis

We previously defined the internal states of the system as $\boldsymbol{x} = [\tilde{\boldsymbol{q}} - \boldsymbol{q}, \boldsymbol{\omega}, \boldsymbol{q}, 1]$ and we write the constraints as matrix inequalities of the form $\boldsymbol{x}^T A\boldsymbol{x} \geq 0$ (VII.D).

Now for the stability criterion (7) we can say that outside the zero state set $\boldsymbol{x}^T A_1\boldsymbol{x} \geq 0$ we have $\boldsymbol{x}^T A_0\boldsymbol{x} \geq 0$. Similarly assuming the same zero-state set for perception map constraints, all the observer constraints hold, i.e. $\boldsymbol{x}^T A_i\boldsymbol{x} \geq 0$ for $i = 2, \cdot, \cdot, \cdot, 6$. Hence we require that,

$$\boldsymbol{x}^T A_i\boldsymbol{x}^T \geq 0 \Rightarrow \boldsymbol{x}^T A_0\boldsymbol{x} \geq 0 \quad \text{ for } i = 1, \cdot, \cdot, \cdot, 6$$

Here we can use S-Procedure and eliminate the state $\boldsymbol{x}$ and write the inequality in the form of a LMI for some $\lambda_i > 0$, as

$$A = A_0 - \lambda_1 A_1 - \lambda_2 A_2 - \lambda_3 A_3 - \lambda_4 A_4 - \lambda_5 A_5 - \lambda_6 A_6 \geq 0 \ , \tag{13}$$

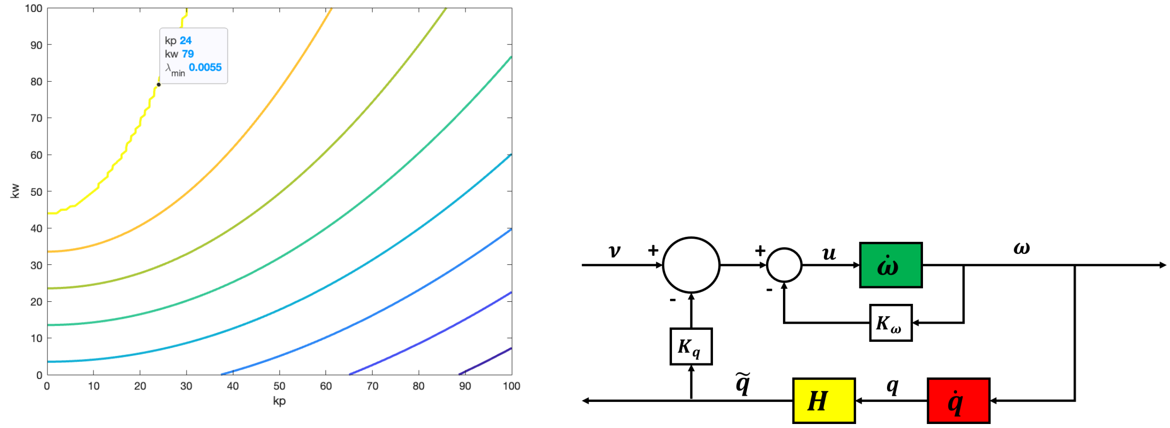

(a) (b)

Figure 5 :(a) Feasible set shown within the lowest level set (yellow) $A \geq 0$. The controller gains within the set shown in yellow correspond case where lowest eigenvalue of A is greater than 0, and is therefore PSD. (b)System diagram showing the attitude rate subsystem which is strictly passive and the matrix subsystem with perception map that is generalized passive.

where,

$$A = \left[\begin{array}{c|c|c|c} \lambda_5 & k_q/2 & \frac{\lambda_2-\lambda_3}{2} & 0 \\ \hline k_q/2 & k_\omega - \lambda_6 & 0 & 0 \\ \hline \frac{\lambda_2-\lambda_3}{2} & 0 & -\lambda_1 - \lambda_2(\beta-1) - \lambda_3(1-\alpha) + \lambda_4 & 0 \\ \hline 0 & 0 & 0 & \lambda_1\epsilon - \lambda_4\gamma - \lambda_5\delta + \lambda_6\Omega \end{array}\right] \geq 0 \tag{14}$$

Thus for a robust controller $\boldsymbol{u} = -k_q\tilde{\boldsymbol{q}} - k_\omega\boldsymbol{\omega}$ we need A to be a positive semi-definite matrix. Also note here that A is a function of controller gains k_q, k_ω for some feasible λ_i's. Here we use an SDP solver to characterize a feasible set of λ_is and derive at a set of feasible values for control gains for these λ_is.

The feasible sets of PSD matrices as a function of the controller gains is shown in Fig- 5a.

Now we can claim that for the feedback interconnection with $\boldsymbol{u} = -k_q\tilde{\boldsymbol{q}} - k_\omega\boldsymbol{\omega}$ and $A \geq 0$ the system is passive. *Proof*: Take the candidate storage system defined as $V(\boldsymbol{\omega}, \boldsymbol{q}) = V_1(\boldsymbol{\omega}) + k_q V_2(\boldsymbol{q}) = \frac{1}{2}\boldsymbol{\omega}J\boldsymbol{\omega} + 2k_q \ln(1 + \boldsymbol{q}^T\boldsymbol{q})$ with $\boldsymbol{u} = \boldsymbol{\nu} - k_q\tilde{\boldsymbol{q}} - k_\omega\boldsymbol{\omega}$, then differentiating along the trajectories we obtain,

$$\begin{aligned} \dot{V} &= \boldsymbol{\omega}J\dot{\boldsymbol{\omega}} + 4k_q\frac{\boldsymbol{q}^T\dot{\boldsymbol{q}}}{(1+\boldsymbol{q}^T\boldsymbol{q})} \\ &= \boldsymbol{\omega}^T\boldsymbol{u} + k_q\boldsymbol{q}^T\boldsymbol{\omega} \\ &= -k_\omega\boldsymbol{\omega}^T\boldsymbol{\omega} \ - k_q\tilde{\boldsymbol{q}}^T\boldsymbol{\omega} + \boldsymbol{\nu}^T\boldsymbol{\omega} + k_q\boldsymbol{q}^T\boldsymbol{\omega} \\ &= (-k_\omega\boldsymbol{\omega}^T\boldsymbol{\omega} \ - k_q(\tilde{\boldsymbol{q}} - \boldsymbol{q})^T\boldsymbol{\omega}) + \boldsymbol{\nu}^T\boldsymbol{\omega} \\ &\leq \boldsymbol{\nu}^T\boldsymbol{\omega}. \end{aligned}$$

Thus the system as seen in Fig-5b is passive for the input ν and output $\boldsymbol{\omega}$.

D. Zeroth-order optimisation

The previous analysis characterizes a feasible set of controller gains that meet stability and passivity constraints. We can also observe from Eq:(4) that a high gain controller would be feasible with the constraints, but it is undesirable for implementation. For example, high gain controllers give large swings in input torques to the reaction wheels of the spacecraft that could damage the sensitive equipment and reduce operation life of the actuators. Low gain controller, on the other hand, will take longer window of time to stabilize and will use higher energy. Thus we use a quadratic cost that penalizes state error and input energy. Specifically, the cost for initial states $\boldsymbol{q}_0, \omega_0$ is given by:

$$J = \int_0^T \boldsymbol{q}_t^T Q \boldsymbol{q}_t + \omega_t^T W \omega_t + \boldsymbol{u}_t^T R \boldsymbol{u}_t \; dt \tag{15}$$

$$\tag{16}$$

We now pick optimal controller gains minimizing this cost over feasible initial states, such that the passivity and stability constraints are satisfied. Thus the problem can be defined as:

$$\begin{aligned}
\arg_{k_p,k_w} \min_{[\boldsymbol{q}_0 \sim \mathcal{D}(0,\Sigma_q), \omega_0 \sim \mathcal{D}(0,\Sigma_\omega)]} \quad & \int_0^T \boldsymbol{q}_t^T Q \boldsymbol{q}_t + \omega_t^T W \omega_t + \boldsymbol{u}_t^T R \boldsymbol{u}_t \; dt \\
\text{s.t.} \quad & \dot{\boldsymbol{q}}_t = G(\boldsymbol{q}_t)\omega_t \\
& J\dot{\omega}_t = -S(\omega_t) J \omega_t + \boldsymbol{u} \\
& \tilde{\boldsymbol{q}}_t = \mathcal{H}(\boldsymbol{q}_t) \\
& \boldsymbol{u}_t = k_\omega \omega_t + k_q \tilde{\boldsymbol{q}}_t \\
& A \geq 0
\end{aligned}$$

This is a non linear optimization problem where we assume that the time horizon T is larger than time required to stabilize. The initial states $\boldsymbol{q}, \omega$ are sampled from distribution of a feasible initial conditions for the attitude stabilization problem. The last constraint $A \geq 0$ ensures the stability and passivity constraints defined earlier hold.

We now use a zeroth-order optimization [27] method for computing optimal controller gains. The algorithm [1] uses sample based gradient information to iterate over minimising gains k_p, k_ω. We initialise M trajectories with a initial feasible control law $\boldsymbol{u} = K_0 [\omega, \boldsymbol{q}]^T$. For each iteration a cumulative cost is computed for the M trajectories we initialized. The Fig-6a shows the sample space for the cumulative cost which is L-smooth in the region of feasible gains selected here. For a given iteration, we randomly sample controller gains around K_i in a ball of radius r which defined the learning rate. The controller updates in the decreasing gradient direction, similar to a stochastic gradient algorithm. We also iteratively reduce the learning rate r as the iterations converge.

We use the optimal controller gains in the simulation pipeline and the attitude can be observed to have been stabilized to within the zero-state set as seen in Fig-6b.

IV. Multi-agent Consensus

We have established a zeroth-order optimal attitude stabilization system for ego-target tracking problem which is passivity-short under noisy observers. The setup can now be extended from single agent pairing to case of distributed estimation.

We examine a problem setup where multiple ego spacecraft are in orbit around a single uncontrolled target spacecraft. Each of the ego-target pairs has the passivity based attitude stabilisation controller to keep alignment. A fully connected communication network exists between each ego agent and they can share there estimated relative target locations and their own global orientation and position w.r.t. Earth fixed frame.

Denote the measurement derived from consensus on desired ego attitude derived from all agents as $\tilde{\boldsymbol{q}}_c$. We substitute the measurement in our previous analysis and use the control input given by $u_1 = -k_q \tilde{\boldsymbol{q}}_c - k_\omega \boldsymbol{\omega}$.

Thus the stability constraint set can now be written as:

$$\dot{V}_1 = -k_\omega \omega_1^T \omega_1 - k_q (\tilde{\boldsymbol{q}}_c - \boldsymbol{q}_1)^T \omega_1 \; . \tag{17}$$

Algorithm 1 :Naive multi-point Zeroth-order Optimization on constraint set

Initialize $\boldsymbol{x}_0 \sim \mathcal{D}(0, \Sigma), K_0 = [k_q, k_\omega], \epsilon$
while $C_i - C_{i-1} \geq \epsilon$ **do**
  for $j = 1, .., N$ **do**
    $U_j \sim \mathcal{B}_r$ ▷ sample over boundary of norm ball with radius r
    $K_j = K_{i-1} + U_j$ ▷ re-sample if K_i is infeasible
    for $t = 0, .., T$ **do** ▷ repeat for M trajectories

$$u_t = -K^T \begin{bmatrix} \tilde{\boldsymbol{q}}_t \\ \omega_t \end{bmatrix}$$

$$\dot{\boldsymbol{q}}_t = G(\boldsymbol{q}_t)\omega_t$$
$$J\dot{\omega}_t = -S(\omega_t)J\omega_t + \boldsymbol{u}_t$$

$$C_j = C_j + \boldsymbol{q}_t^T Q \boldsymbol{q}_t + \omega_t^T W \omega_t + u_t^T R u_t$$

    end for
    $C_i = \min C_j$
    $K_i \longrightarrow \arg\min_{K_j} C_j$
    $i = i + 1$
  end for
end while

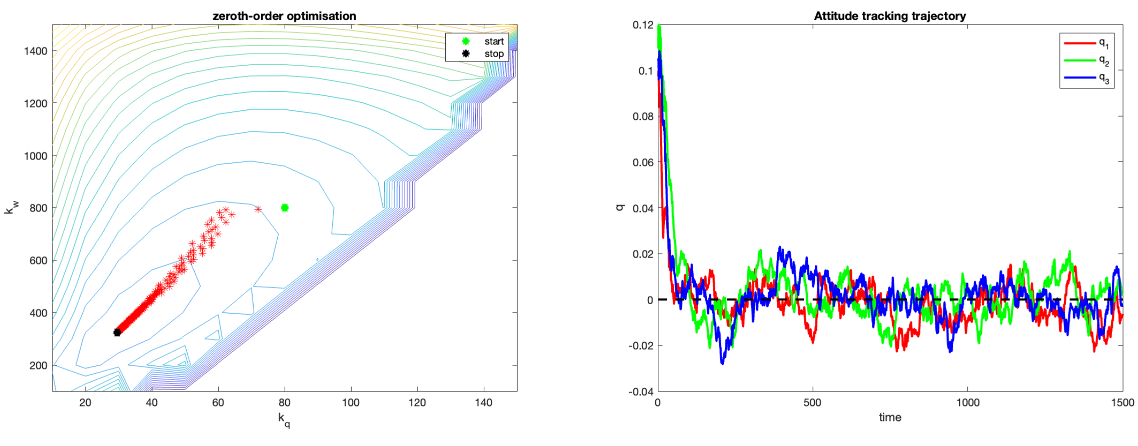

(a) **(b)**

Figure 6 :(a) Quadratic cost on a set of trajectories initialized from $x_0 \sim \mathcal{D}(0, \Sigma)$. The trajectories are simulated for a time horizon T with passivity based control law and ML based estimation. For feasible sets of control gains we obtain an L-smooth mapping from gains to the cost function. Here we also show iterative updates of Zeroth-order optimization. The plot shows infeasible region on the bottom right. The initial control gain shown in green and optimal controller in black and iterations are plotted in red. (b) Attitude trajectory under noisy observation. The MRP attitude states are stabilized to a reference $[0, 0, 0]$ i.e., camera center.

Using the setup for feasibility analysis we can replace $\tilde{\boldsymbol{q}}_1$ with $\tilde{\boldsymbol{q}}_c$ by giving reduced bounds on $\tilde{\boldsymbol{q}}_c - \boldsymbol{q}_1$. The constraints from section III.B follow here with $\tilde{\boldsymbol{q}}_c$ with new sector bounds α', β' and new error bound δ' and new feasibility set is defined such that $A' \geq 0$. Tighter bounds increase the size of the feasible control set and we can design a controller for a stricter quadratic cost by weighting the control penalty lower to achieve an aggressive controller, which is currently not achievable as larger feasible set limits aggressive control. Design of the consensus based controller can now be achieved using the same procedure discussed from section II.D-III.D by replacing $\tilde{\boldsymbol{q}}_1$ with $\tilde{\boldsymbol{q}}_c$.

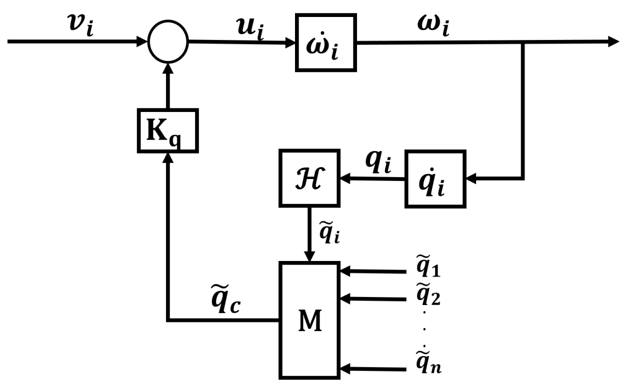

Figure 7 :Feedback interconnection of multi-agent ego-target systems. Here system i is the primary ego-target pair. Measurements from all n passive agents are used as feedback to system i. The mixing matrix M is representation for consensus based measurement $\tilde{q}_c$.

A. Weighted Averaging Consensus approach

We define relative ego attitude measurement for first ego-target pair as $\tilde{\boldsymbol{q}}_1$, and the information shared from neighboring ego spacecrafts in the frame of reference of the first spacecraft as $\tilde{\boldsymbol{q}}_2, \cdot, \cdot, \tilde{\boldsymbol{q}}_n$ for n agents. Taking a weighted average for observation on the ego attitude we can write:

$$\tilde{\boldsymbol{q}}_{\text{avg}} = \frac{1}{n}\sum_{i=1}^{n} \alpha_i \tilde{\boldsymbol{q}}_i \tag{18}$$

This sum converges to a weighted mean in the convex hull defined by $\tilde{\boldsymbol{q}}_i$, for $\alpha_i > 0\ \forall i$ and $\sum \alpha_i = 1$.* In the scenario where the confidence on a measurement of a single agent is significantly higher than others we would prefer to trust that particular measurement as opposed to an average of all measurements. Thus we also look at a max consensus approach.

B. Dynamic Max consensus protocol

We show use of a max consensus protocol in distributed pose estimation. The averaging consensus can not offer analytical bounds on deviation from true state as we are using a sector bounded error model with non-Gaussian distribution. Using weighting in averaging we give more emphasis to agents with higher confidence in their measurements. This max consensus is a sort of variation on weighted averaging where we pick only measurement with highest confidence as the observation.

Here we use a confidence parameter α_j on the relative distance measurements made by CNN in j^{th} ego's frame. Transforming the measurement to i^{th} agent, the measurements become $\boldsymbol{q}_{ij} = \mathcal{F}_{ij}(\boldsymbol{q}_j)$ (the mapping is shown in section VII.C). Now we do a consensus on max confidence for each agent and pick the measurement with the highest confidence, namely,

$$\tilde{\boldsymbol{q}}_i = \tilde{\boldsymbol{q}}_{ij} \quad \text{where} \quad j = \arg \max_{\forall j \in \{1,2,..,n\}} \alpha_j \tag{19}$$

This consensus methodology applies for different network configurations.

V. Simulation and Numerical Experiment

The simulation setup used here is based on a multi-agent ego-target tracking problem. We initiate a trajectory for a tumbling target satellite with six ego agents in passive relatively elliptical orbits around the target. The relative orbits of each ego agent are shown in Fig- 8a. The ego satellites have a camera attached to the body x-axis and are independently tracking the target using the passivity based controller. The onboard attitude and angular velocity estimation is done

*Other averaging schemes that are consistent with the geometry of MRPs can also be considered

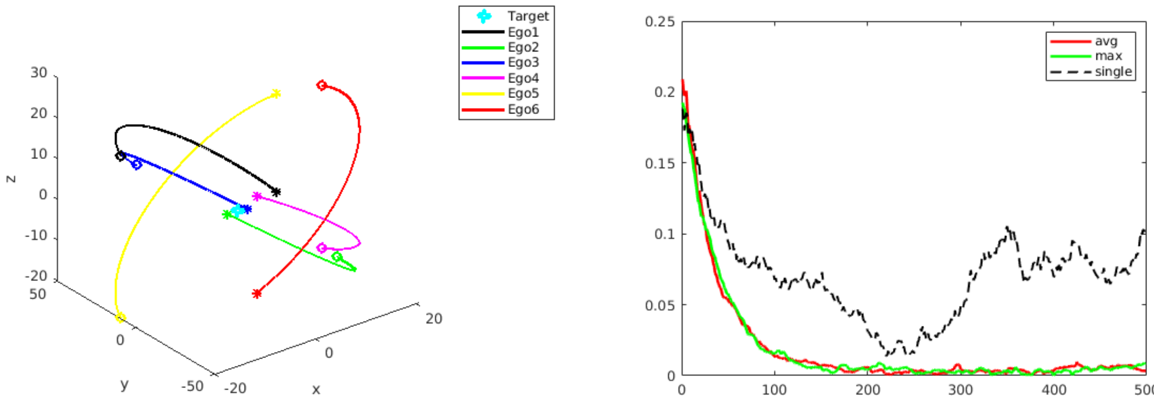

(a) **(b)**

Figure 8 :(a)ego trajectories around target shown in blue(b)Comparison of attitude tracking error over a trajectory. Tracking for an agent with poor estimation without consensus compared to weighted averaging and max consensus based estimation

through an EKF under the assumption of Gaussian measurement noise for the states. The details of assumptions on EKF filter are listed in section VII.B.

The multi-agent setup is simulated under a fully connected network thus all agents communicate their state and measurement information to every other agent in global reference frame. Each of the ego spacecrafts then convert the relative target information in their own respective body frame as shown in section VII.C. Further details of the simulation framework are given in [24]

VI. Conclusion

We presented a passivity based controller under non-linear observations synthesized from machine learning based algorithms. The problem setup we analyzed was aimed at solving the ego-target satellite tracking using only a single camera. Works presented in [24] discuss the ML based algorithms we use for estimation and the simulation framework based on Unreal Engine to produce photo-realistic visualisation and inputs.

The characteristics of our CNN based estimator are represented as sector bounded non-linearity. This modelling gives us a passivity-short framework and we define the controller that works in a region defined by all feasible attitude trajectories for the ego-target pair. Among the set of feasible controllers we pick an optimal controller that minimizes input energy and tracking error using a zeroth-order optimization approach from the data gathered through our simulation engine.

The passive nature of the system allows us to extend the framework to multi-agent setup for passive systems. We use a consensus based estimation from each agents, CNN based measurement. Using passivity properties of each agent we ensure that feedback interconnection remains passive and the controller setup can be extended to the consensus case.

We demonstrate the use of a weighted averaging and a max-consensus algorithms based on confidence parameters assigned to the measurements by the perception map. The consensus algorithms show reduced tracking errors under the same controller due to better estimation. In this work, we only look at a centralized approach using feedback from each agent in the network. The likely future direction would evaluate a distributed controller.

Extensions to this work include generalized controller for a broader domain of passivity short systems with sector bounded non-linearities. Moreover adaptive controllers that can exploit state dependence of errors models for CNN-based measurement are a pertinent future direction for this work.

VII. Appendix

We provide a definitions of passivity pertaining to this work.

A. Passivity Theorems

Consider the dynamical system [16]:

$$\dot{\boldsymbol{x}} = f(\boldsymbol{x}, \boldsymbol{u}) \tag{20}$$

$$\boldsymbol{y} = h(\boldsymbol{x}, \boldsymbol{u}) \tag{21}$$

where $f : \mathbb{R}^n \times \mathbb{R}^p \to \mathbb{R}^n$ is locally Lipschitz, $h : \mathbb{R}^n \times \mathbb{R}^p \to \mathbb{R}^p$ is continuous, $f(0,0) = 0$, and $h(0,0) = 0$.

Definition 3. *The system VII.A is said to be zero state observable if no solution of $\dot{\boldsymbol{x}} = f(\boldsymbol{x}, \boldsymbol{u})$ can stay identically in the set $S = \{h(\boldsymbol{x}, 0) = 0\}$, other than zero solution $\boldsymbol{x}(t) = 0$*

Definition 4. *The system VII.A is said to be passive if there exists a continuously differentiable non-negative function $V(\boldsymbol{x})$, called the storage function, such that*

$$\boldsymbol{u}^T \boldsymbol{y} \geq \dot{V} = \frac{\partial V}{\partial \boldsymbol{x}} f(\boldsymbol{x}, \boldsymbol{u}), \quad \forall (\boldsymbol{x}, \boldsymbol{u}) \in \mathbb{R}^n \times \mathbb{R}^p \tag{22}$$

Theorem 1. *If system VII.A is*

1) *passive with a radially bounded PD storage function,*
2) *zero-stable observable,*

then the origin $\boldsymbol{x} = 0$ can be globally stabilized by $\boldsymbol{u} = -\phi(\boldsymbol{x})$, where ϕ is any locally Lipschitz function such that $\phi(0) = 0$ and $\boldsymbol{y}^T \phi(\boldsymbol{y}) > 0$ for all $\boldsymbol{y} \neq 0$. Here f is locally Lipschitz in $(\boldsymbol{x}, \boldsymbol{u})$ and h is continuous is $\boldsymbol{x}$

B. Simulation with Noisy measurements

Assumptions for the Ego state estimation:

- An EKF-type filter has been applied for state estimation on board each ego spacecraft system:

$$x_k = f(x_{k-1}) + w_{k-1}$$
$$z_k = h(x_k) + v_k$$

  ignoring the perception error.
- Here w_k and v_k are temporally uncorrelated (white noise), zero-mean random sequences with known co-variances and both uncorrelated with the initial state. Thus using EKF we state that if,
    1) $\alpha, \beta, \gamma_1, \gamma_2 > 0$ are positive reals for each $k > 0$:

$$||J_f(x_k)|| \leq \alpha$$
$$||J_h(x_k)|| \leq \beta$$
$$\gamma_1 I \leq P_k \leq \gamma_2 I$$

    2) J_r is non singular for all k
    3) There are positive real numbers $\epsilon_\phi, \epsilon_\chi, \kappa_\phi, \kappa_\chi > 0$ such that:

$$||\phi(x_k, \hat{x_k})|| \leq \epsilon_\phi ||x_k - \hat{x_k})||^2 \quad \text{with} \quad ||x_k - \hat{x_k})|| \leq \kappa_\phi$$
$$||\chi(x_k, \hat{x_k})|| \leq \epsilon_\chi ||x_k - \hat{x_k})||^2 \quad \text{with} \quad ||x_k - \hat{x_k})|| \leq \kappa_\chi \quad ,$$

  then the **estimation error is bounded exponentially** given that the initial estimation error is bounded [28].

C. Transformation mapping

For each ego agent j, we have a perception map measurement of relative target distance as $\tilde{r}_j$. The rotation with respect to ECEF is given by $\hat{R}_j$ (in SO3) and the position with respect to ECEF is $\hat{e}_j$. The transformation of relative target measurement from ego j to ego frame of i is given by:

$$
\begin{aligned}
\tilde{\boldsymbol{r}}_{ij} &= \hat{R}_i(\hat{\boldsymbol{e}}_j + \hat{R}_j^{-1}\tilde{\boldsymbol{r}}_j - \hat{\boldsymbol{e}}_i) \\
\tilde{\boldsymbol{r}}_{ij} &= \hat{R}_i(\hat{\boldsymbol{e}}_j - \hat{\boldsymbol{e}}_i + \hat{R}_j^{-1}\tilde{\boldsymbol{r}}_i) \\
\tilde{\boldsymbol{r}}_{ij} &= \hat{R}_i(\hat{\boldsymbol{d}}_{ji} + \hat{R}_j^{-1}\tilde{\boldsymbol{r}}_i) \\
\tilde{\boldsymbol{r}}_{ij} &= \hat{R}_i\hat{\boldsymbol{d}}_{ji} + \hat{R}_i\hat{R}_j^{-1}\tilde{\boldsymbol{r}}_i
\end{aligned}
$$

Given the relative distance of target from ego in the body frame we compute desired ego attitude for tracking the target to align with ego's camera axis($\boldsymbol{x}$-axis: $\boldsymbol{x} = [1, 0, 0]$):

$$
\begin{aligned}
\boldsymbol{p} &= \frac{\tilde{\boldsymbol{r}}_{ij}}{|\tilde{\boldsymbol{r}}_{ij}|} \\
\boldsymbol{s} &= \boldsymbol{x} \times \boldsymbol{p} \\
\hat{\boldsymbol{s}} &= \frac{\boldsymbol{s}}{|\boldsymbol{s}|} \\
\theta &= \cos^{-1}(\langle \boldsymbol{x}, \boldsymbol{p} \rangle) \\
\tilde{\boldsymbol{q}}_{ij} &= \hat{\boldsymbol{s}} \tan(\frac{\theta}{4})
\end{aligned}
$$

D. Constraint sets

Constraint set		
Stability $\dot{V} \leq 0$	$k_\omega \omega^T \omega + k_q (\tilde{q} - q)^T \omega \geq 0$	$x^T A_0 x \geq 0, \quad A_0 = \begin{bmatrix} 0 & k_q/2 & 0 & 0 \\ k_q/2 & k_\omega & 0 & 0 \\ 0 & 0 & 0 & 0 \\ 0 & 0 & 0 & 0 \end{bmatrix}$
Avoiding Zero-state set	$\|\|q\|\| \leq \epsilon$	$x^T A_1 x \geq 0, \quad A_1 = \begin{bmatrix} 0 & 0 & 0 & 0 \\ 0 & 0 & 0 & 0 \\ 0 & 0 & 1 & 0 \\ 0 & 0 & 0 & -\epsilon \end{bmatrix}$
Avoiding Zero-state set	$\|\|\omega\|\| \leq \Omega$	$x^T A_2 x \geq 0, \quad A_2 = \begin{bmatrix} 0 & 0 & 0 & 0 \\ 0 & 1 & 0 & 0 \\ 0 & 0 & 0 & 0 \\ 0 & 0 & 0 & -\Omega \end{bmatrix}$
Sector upper Bounds	$\beta q^T q \geq \tilde{q}^T q$ $\beta q^T q - \tilde{q}^T q + q^T q - q^T q \geq 0$ $-(\tilde{q} - q)^T q + (\beta - 1) q^T q \geq 0$	$x^T A_3 x \geq 0, \quad A_3 = \begin{bmatrix} 0 & 0 & -1/2 & 0 \\ 0 & 0 & 0 & 0 \\ -1/2 & 0 & \beta - 1 & 0 \\ 0 & 0 & 0 & 0 \end{bmatrix}$
Sector lower Bounds	$\beta q^T q \geq \tilde{q}^T q \geq \alpha q^T q$ $\tilde{q}^T q - \alpha q^T q + q^T q - q^T q \geq 0$ $(\tilde{q} - q)^T q + (1 - \alpha) q^T q \geq 0$	$x^T A_4 x \geq 0, \quad A_4 = \begin{bmatrix} 0 & 0 & 1/2 & 0 \\ 0 & 0 & 0 & 0 \\ 1/2 & 0 & 1 - \alpha & 0 \\ 0 & 0 & 0 & 0 \end{bmatrix}$
State Upper Bounds	$\|\|q\|\| \leq \gamma$	$x^T A_5 x \geq 0, \quad A_5 = \begin{bmatrix} 0 & 0 & 0 & 0 \\ 0 & 0 & 0 & 0 \\ 0 & 0 & -1 & 0 \\ 0 & 0 & 0 & \gamma \end{bmatrix}$
Error Upper Bounds	$\|\|\tilde{q} - q\|\| \leq \delta$	$x^T A_6 x \geq 0, \quad A_6 = \begin{bmatrix} -1 & 0 & 0 & 0 \\ 0 & 0 & 0 & 0 \\ 0 & 0 & 0 & 0 \\ 0 & 0 & 0 & \delta \end{bmatrix}$

Acknowledgements

Part of this research was carried out at the Jet Propulsion Laboratory, California Institute of Technology, under a contract with the National Aeronautics and Space Administration.

References

[1] Guglieri, G., Maroglio, F., Pellegrino, P., and Torre, L., "Design and Development of Guidance Navigation and Control Algorithms for Spacecraft Rendezvous and Docking Experimentation," *Acta Astronautica*, Vol. 94, No. 1, 2014, pp. 395–408. https://doi.org/https://doi.org/10.1016/j.actaastro.2013.02.010, URL https://www.sciencedirect.com/science/article/pii/S0094576513000581.

[2] Filipe, N., and Tsiotras, P., "Adaptive Position and Attitude-Tracking Controller for Satellite Proximity Operations Using Dual Quaternions," *Journal of Guidance, Control, and Dynamics*, Vol. 38, No. 4, 2015, pp. 566–577. https://doi.org/10.2514/1.G000054, URL https://doi.org/10.2514/1.G000054.

[3] Xiang, Y., Schmidt, T., Narayanan, V., and Fox, D., "PoseCNN: A Convolutional Neural Network for 6D Object Pose Estimation in Cluttered Scenes," *CoRR*, Vol. abs/1711.00199, 2017. URL http://arxiv.org/abs/1711.00199.

[4] Hu, Y., Hugonot, J., Fua, P., and Salzmann, M., "Segmentation-driven 6D Object Pose Estimation," *CVPR*, 2019, p. 1.

[5] Kisantal, M., Sharma, S., Park, T. H., Izzo, D., Märtens, M., and D'Amico, S., "Satellite Pose Estimation Challenge: Dataset, Competition Design, and Results," *IEEE Transactions on Aerospace and Electronic Systems*, Vol. 56, No. 5, 2020, pp. 4083–4098. https://doi.org/10.1109/TAES.2020.2989063.

[6] Clohessy, W., and Wiltshire, R., "Terminal Guidance System for Satellite Rendezvous," *Journal of the Aerospace Sciences*, Vol. 27, No. 9, 1960, pp. 653–658. https://doi.org/10.2514/8.8704.

[7] Alfriend, K. T., Vadali, S. R., Gurfil, P., How, J. P., and Breger, L. S., *Chapter 5 - Linear Equations of Relative Motion*, Butterworth-Heinemann, Oxford, 2010. https://doi.org/https://doi.org/10.1016/B978-0-7506-8533-7.00210-4, URL https://www.sciencedirect.com/science/article/pii/B9780750685337002104.

[8] Silani, E., and Lovera, M., "Magnetic Spacecraft Attitude Control: a Survey and Some New Results," *Control Engineering Practice*, Vol. 13, No. 3, 2005, pp. 357–371. https://doi.org/https://doi.org/10.1016/j.conengprac.2003.12.017, URL https://www.sciencedirect.com/science/article/pii/S0967066103002922, aerospace IFAC 2002.

[9] Nasrolahi, S. S., and Abdollahi, F., "Lyapunov Stability Analysis for Non-Linear Satellite Attitude Control in the Presence of States Measurement Error," *2016 4th International Conference on Control, Instrumentation, and Automation (ICCIA)*, 2016, pp. 64–68. https://doi.org/10.1109/ICCIAutom.2016.7483137.

[10] Tsiotras, P., "Stabilization and Optimality Results for the Attitude Control Problem," *Journal of Guidance, Control, and Dynamics*, Vol. 19, No. 4, 1996, pp. 772–779. https://doi.org/10.2514/3.21698, URL https://doi.org/10.2514/3.21698.

[11] Tsiotras, P., "Optimal Regulation and Passivity Results for Axisymmetric Rigid Bodies Using Two Controls," *Journal of Guidance, Control, and Dynamics*, Vol. 20, No. 3, 1997, pp. 457–463. https://doi.org/10.2514/2.4097, URL https://doi.org/10.2514/2.4097.

[12] Tsiotras, P., "Further Passivity Results for the Attitude Control Problem," *IEEE Transactions on Automatic Control*, Vol. 43, No. 11, 1998, pp. 1597–1600. https://doi.org/10.1109/9.728877.

[13] Erdong, J., and Zhaowei, S., "Passivity-Based Control for a Flexible Spacecraft in the Presence of Disturbances," *International Journal of Non-Linear Mechanics*, Vol. 45, No. 4, 2010, pp. 348–356. https://doi.org/https://doi.org/10.1016/j.ijnonlinmec.2009.12.008, URL https://www.sciencedirect.com/science/article/pii/S0020746209002224.

[14] Lei, J., "Passivity-Based Output Feedback Control for Systems With Nonlinear Outputs Via High-Gain Observers," *Journal of Dynamic Systems, Measurement, and Control*, Vol. 144, No. 4, 2022. https://doi.org/10.1115/1.4053140, URL https://doi.org/10.1115/1.4053140, 041002.

[15] Tsiotras, P., "Stabilization and Optimality Results for the Attitude Control Problem," *Journal of Guidance, Control, and Dynamics*, Vol. 19, No. 4, 1996, pp. 772–779. https://doi.org/10.2514/3.21698, URL https://doi.org/10.2514/3.21698.

[16] Khalil, H., *Nonlinear Systems*, Pearson Education, Prentice Hall, 2002.

[17] Rahimi, N., Talebi, S., Deole, A., Mesbahi, M., Bandyopadhyay, S., and Rahmani, A., *Robust Controller Synthesis for Vision-based Spacecraft Guidance and Control*, AIAA, 2022. https://doi.org/10.2514/6.2022-2213, URL https://arc.aiaa.org/doi/abs/10.2514/6.2022-2213.

[18] Fazlyab, M., Morari, M., and Pappas, G. J., "Probabilistic Verification and Reachability Analysis of Neural Networks via Semidefinite Programming," *Proceedings of the IEEE Conference on Decision and Control*, Vol. 2019-Decem, 2019, pp. 2726–2731. https://doi.org/10.1109/CDC40024.2019.9029310.

[19] Hu, H., Fazlyab, M., Morari, M., and Pappas, G. J., "Reach-SDP: Reachability Analysis of Closed-Loop Systems with Neural Network Controllers via Semidefinite Programming," *arXiv*, 2020, pp. 1–15. https://doi.org/10.1109/cdc42340.2020.9304296.

[20] Fazlya, M., Robey, A., Hassani, H., Morari, M., and Pappas, G. J., "Eficient and Accurate Estimation of Lipschitz Constants for deep neural networks," *arXiv*, , No. NeurIPS, 2019.

[21] Dean, S., Matni, N., Recht, B., and Ye, V., "Robust Guarantees for Perception-Based Control," *Proceedings of the 2nd Conference on Learning for Dynamics and Control*, Proceedings of Machine Learning Research, Vol. 120, edited by A. M. Bayen, A. Jadbabaie, G. Pappas, P. A. Parrilo, B. Recht, C. Tomlin, and M. Zeilinger, PMLR, 2020, pp. 350–360. URL https://proceedings.mlr.press/v120/dean20a.html.

[22] Proença, P. F., and Gao, Y., "Deep Learning for Spacecraft Pose Estimation from Photorealistic Rendering," *CoRR*, Vol. abs/1907.04298, 2019. URL http://arxiv.org/abs/1907.04298.

[23] Chen, B., Cao, J., Bustos, Á. P., and Chin, T., "Satellite Pose Estimation with Deep Landmark Regression and Nonlinear Pose Refinement," *CoRR*, Vol. abs/1908.11542, 2019. URL http://arxiv.org/abs/1908.11542.

[24] Becktor, J., Seto, W., Deole, A., Bandyopadhyay, S., Rahimi, N., Talebi, S., Mesbahi, M., and Rahmani, A., "Robust Vision-based Multi-spacecraft Guidance Navigation and Control using CNN-based Pose Estimation," *2022 IEEE Aerospace Conference (AERO)*, 2022, pp. 1–10. https://doi.org/10.1109/AERO53065.2022.9843396.

[25] Kenneally, P. W., Piggott, S., and Schaub, H., "Basilisk: A Flexible, Scalable and Modular Astrodynamics Simulation Framework," *Journal of Aerospace Information Systems*, Vol. 17, No. 9, 2020, pp. 496–507. https://doi.org/10.2514/1.I010762, URL https://doi.org/10.2514/1.I010762.

[26] Egeland, O., and Godhavn, J.-M., "Passivity-Based Adaptive Attitude Control of a Rigid Spacecraft," *IEEE Transactions on Automatic Control*, Vol. 39, No. 4, 1994, pp. 842–846. https://doi.org/10.1109/9.286266.

[27] Liu, S., Chen, P.-Y., Kailkhura, B., Zhang, G., Hero III, A. O., and Varshney, P. K., "A Primer on Zeroth-Order Optimization in Signal Processing and Machine Learning: Principals, Recent Advances, and Applications," *IEEE Signal Processing Magazine*, Vol. 37, No. 5, 2020, pp. 43–54. https://doi.org/10.1109/MSP.2020.3003837.

[28] Reif, K., Gunther, S., Yaz, E., and Unbehauen, R., "Stochastic stability of the Discrete-Time Extended Kalman Filter," *IEEE Transactions on Automatic Control*, Vol. 44, No. 4, 1999, pp. 714–728. https://doi.org/10.1109/9.754809.